Rev. Adv. Mater. Sci. 50 (2017) 13-23

# MICROSTRUCTURE AND MECHANICAL CHARACTERISTICS OF NANOSTRUCTURED NICKEL-GRAPHENE COMPOSITES PROCESSED BY HIGH PRESSURE TORSION

**I.Yu. Archakov[1,2], V.U. Kazykhanov[3], V.G. Konakov[1,4], O.Yu. Kurapova[1,4], A.E. Medvedev[3], M.Yu. Murashkin[3], N.N. Novik[1,4], I.A. Ovid'ko, E. N. Solovyeva[5] and R.Z. Valiev[3]**

[1]Peter the Great St Petersburg Polytechnic University, St. Petersburg 195251, Russia
[2]Institute for Problems of Mechanical Engineering, Russian Academy of Sciences, St Petersburg, 199178, Russia
[3]Institute of Physics of Advanced Materials, Ufa State Aviation Technical University, Ufa 450008, Russia
[4]St. Petersburg State University, St. Petersburg 199034, Russia
[5]Glass and Ceramics Ltd, St Petersburg, 199004, Russia

*Received: October 22, 2016*

**Abstract.** This paper presents data on fabrication of “nickel-graphene-graphite” bulk composites using powder metallurgy methods combined with the high energy ball milling. The composites were then processed by high pressure torsion (HPT) at temperatures of 23 and 200 °C. This treatment gives rise to the formation of new “nanostructured nickel-graphene” composites. The phase composition of the new composite specimens was examined by X-ray diffraction. Raman spectroscopy proved graphite-to-graphene conversion under mechanical treatments. The microstructure of the new composite specimens was investigated by scanning electron and transmission electron microscopy methods. Composite specimens after HPT at temperature of 200 °C demonstrate the optimal combination of strength ($\sigma_{02}$= 923 MPa; $\sigma_b$= 992 MPa) and ductility ($\delta$ = 99%). Composite specimens with 2 wt.% graphene content after HPT at room temperature exhibits superior microhardness $H_v$ = 6.45 GPa.

## 1. INTRODUCTION

Nickel- and nickel-alloy-matrix composites containing inclusions of carbon in its various allotropic modifications exhibit excellent mechanical and functional properties being of high interest for automobile and aerospace industries [1,2]. Typical inclusions of such a type are carbides [3,4], diamond powder [5,6], and carbon nanotubes [7,8]. Nickel-based composite coatings are widely exploited in various applications, while the use of bulk nickel-based composites is limited due to their high brittleness. On the other hand, some technical tasks require bulk nickel-matrix composites with functional combination of mechanical characteristics.

High pressure torsion (HPT) technique is the effective tool for enhancement of the mechanical properties of bulk materials [9]. HTP processing under the defined optimal conditions (number of turns, temperature of torsion) allows ultrafine grain (UFG) structure formation composed of grains having high angle grain boundaries. That results in significant material hardening. In the recent work [9], bulk nickel-

Corresponding author: V. G. Konakov, e-mail: glasscer@yandex.ru

based materials were HPT treated at the temperatures -196 – 400 °C. It was shown that the tensile strength of HPT-treated materials increased from 1000 to 1700 MPa with the increase in carbon content from 0.008 to 0.06 wt.%; it was also stated that carbon addition does not reduce ductility of the material.

Recent studies in the field of metallic matrix composites (Ni, Al, Cu) [1,10] showed that nanotubes are not effective as a carbon dopant because of their high agglomeration and, as a result, low distribution uniformity in the metallic matrix. On the other hand, see [11,12], the incorporation of such carbon-containing additives as graphene, graphene flakes or reduced graphene oxide are prospective for the mechanical properties enhancement. Indeed, graphene is two-dimensional (2D) material formed by $sp^2$-hybridized carbon layers packed in honey comb lattice. It has an outstanding hardness, heat conductivity, high chemical stability, and high surface area. 2D structure is an obvious advantage of graphene over the other allotropic forms of carbon, by which it can be embedded into grain boundaries phase and tends to form mostly monolayer on the grain surface of metallic matrix. It favors to the decrease in the impurities effects and their segregation in the phase boundaries [13]. High energy ball milling of starting materials and further use of powder metallurgy technique, suggested by authors in [14] is a simple and effective way for graphene or graphene flakes doped metallic matrix composites manufacturing. It is expected that HPT treatment of bulk nickel composites doped by graphene-graphite mixture would allow significant enhancement of their mechanical properties. Thus, the goal of the present work is to fabricate bulk nickel-graphene-graphite composites by powder metallurgy technique, their HPT treatment at room temperature and 200 °C and the investigation of phase composition, microstructure, and mechanical properties of the obtained composites before and after HPT treatment.

## 2. EXPERIMENTAL

Commercial fine-grained nickel powder and thermally expanded graphite (TEG) were used for specimen synthesis. In order to diminish the average grain size and to remove possible agglomerates, nickel powder was preliminary meshed using 40 μm sieve. Particle size distribution 'by size' obtained from PSD-analysis (Horiba LA-950) is shown in Fig. 1, as seen from the figure, the mean particle size in the powder is 9 μm.

Pure nickel with no TEG addition corresponds to Specimen I. Different amount of TEG (0.5-2 wt.%) was added to the sieved nickel powder in order to obtain following compositions (wt.%): 99.5Ni-0.5TEG, 99Ni-1TEG, 98Ni-2TEG being Specimens II, III, IV, respectively. Thus prepared mixtures were grinded in a planetary mill (Pulverisette 6) at 450 rpm for 5 hours. Mechanically activated powders were cold pressed into pellets of 30 mm in the diameter and 15 mm in height under the pressure of 5000 kg/cm$^2$ at room temperature (RT). As a result, tablet-like specimens were fabricated. Specimens were annealed at 1250 °C for 1 hour (heating rate 10 °C/min, cooling with the furnace ~ 6 hours down to 500 °C) in a vacuum furnace with the residual pressure less than 0.003 atm. Phase composition

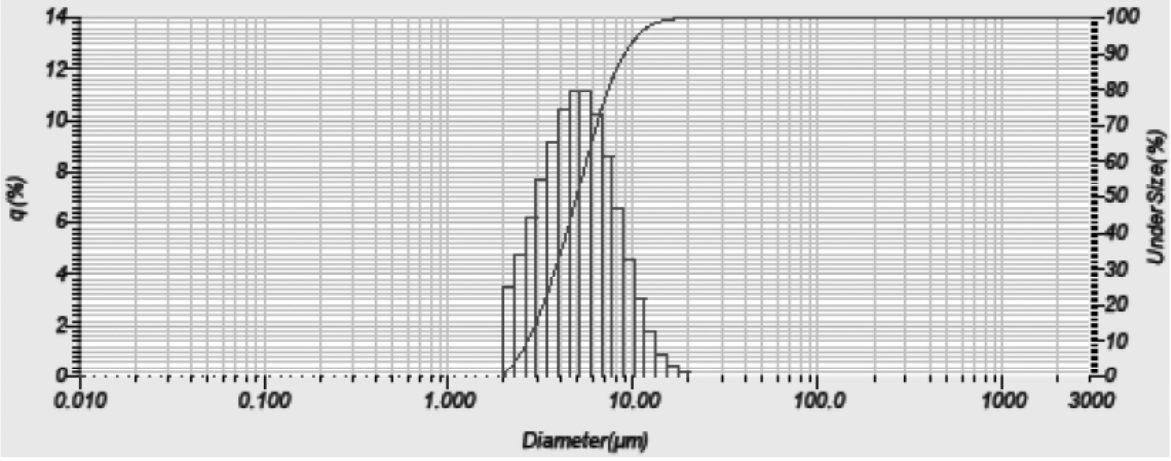


**Fig. 1.** Particle size distribution "by size" in the sieved nickel powder.

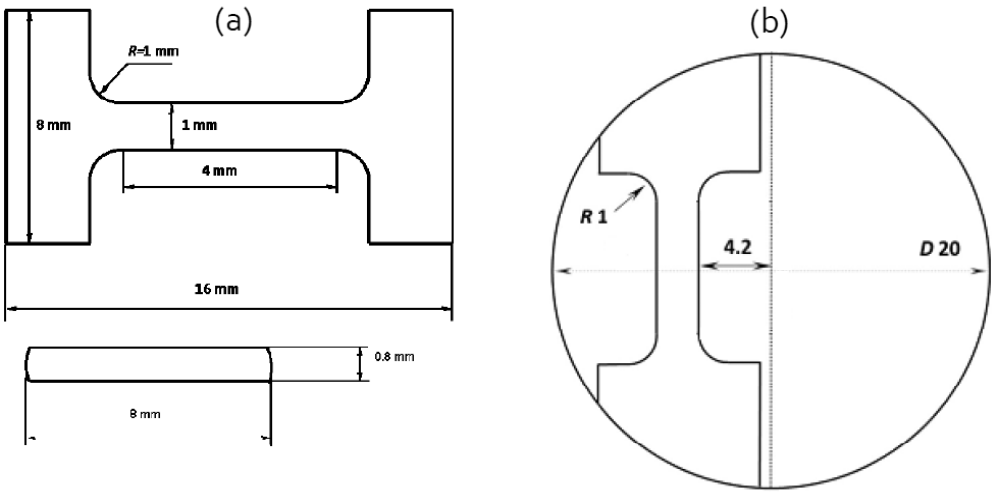


**Fig. 2.** (a) The geometry of the sample for strain tests, (b) the schematic illustration of sample machining after HPT.

of samples was identified via X-Ray diffraction technique (XRD, SHIMADZU XRD-6000, Cu-K$\alpha$, $\lambda$ = 1.54 Å). Corresponding allotropic form of the carbon in the specimens was identified via Raman Spectroscopy (SENTERRA T64000, exciting radiation wave length 488 nm, gate voltage- 40 V). Cylinder shape specimens of 20 mm in diameter were machined by electric discharge cutting technique (ARTA 120 machine) from the final tablet-like specimens. Then the disc-shaped samples with the thickness of 14 mm were obtained from these cylinders. These disc-shaped samples were HPT-treated (SCRUGE 200, $P$ = 6 GPa, $N$=10) at RT and at 200 °C. Number of turns ($N$) was chosen according [15,16] where structural characteristics and materials hardness after HPT were shown to reach saturation level at $N$, corresponding to shear strain ($\gamma$), calculated according to Eq. (1):

$$\gamma = \frac{2\pi RN}{t} . \quad (1)$$

Specimens microstructure was analyzed by transmission electron microscopy (TEM, JEM-2100, JEOL, accelerating voltage 200 keV) in the dark-field and bright-field visualization regimes. Note that specimens were pre-thinned mechanically here in order to reach proper electron-transparence. Electron diffraction images were obtained using the aperture with the nominal diameter of 1 - 10 $\mu$m. Qualitative elemental analysis of thin foil surface was performed by the energy-dispersive X-ray spectroscopy (EDX, Oxford Instruments). The analysis of surface microstructure before and after HPT, as well as fractured surface after the mechanical tests was performed using scanning electron microscopy (SEM, JEOL JSM 6490 LV with the tungsten cathode). Vickers hardness (Hv) was determined at the load of ~3 N applied for 15 seconds (Micromet–5101, diamond pyramid shaped indenter). The data for each specimen is averaged over 15 tests.

Strain tests were carried out using Instron 5982 machine with the deformation rate of $10^{-3}$ $sec^{-1}$ at RT, see [17]. Stress-strain diagrams were plotted on the averaged data obtained for five fractured samples. The characteristics of static strength ($\sigma_b$), tensile strength after failure as nominal yield limit ($\sigma_{02}$), and ductility value ($\delta$) were determined on the averaged data of at least two samples having the geometry presented in Fig. 2a [18,19]. Samples for these tests were manufactured by electric discharge cutting technique according to the scheme demonstrated in Fig. 2b. Prior the mechanical tests, the sample surface was polished using diamond paste, the particle size of the abrasive was less than 1 $\mu$m. All microstructural investigations, as well as microhardness tests, strength, and plasticity values of specimens after HPT treatment were performed in the surface regions located at 0.5$R$ distance from the specimen center.

## 3. RESULTS AND DISCUSSION

XRD pattern of Specimen with 2 wt.% content of TEG before (IV1) and after HPT treatment at RT (IV2)

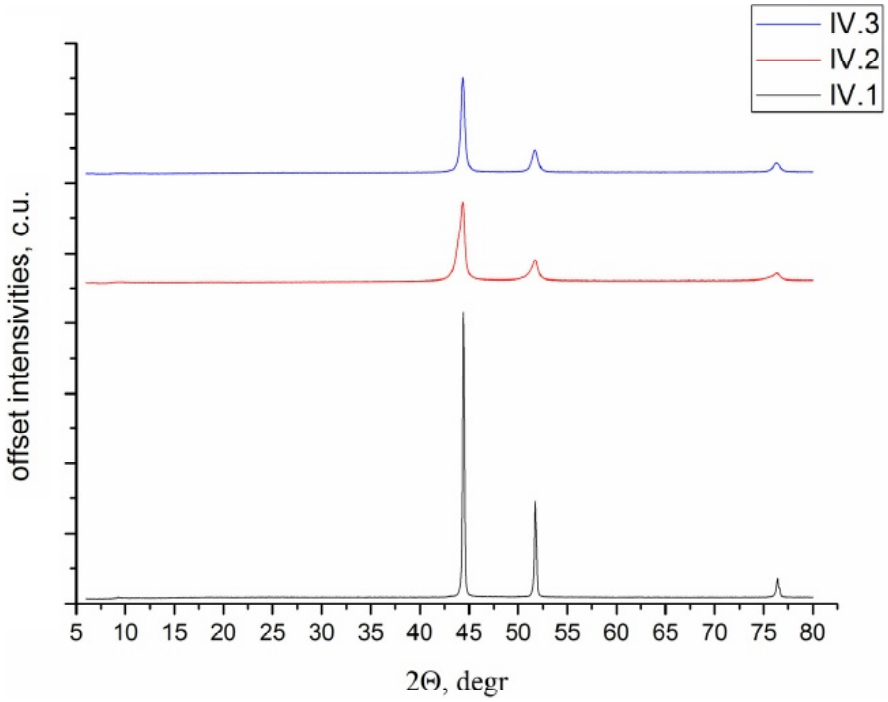


**Fig. 3.** XRD patterns for sample with 2 wt.% graphene-graphite phase content before (IV1) and after HPT at room temperature (IV2) and at 200 °C (IV3).

and at 200 °C (IV3) are shown in Fig. 3. Here and after the same numeration will be used for the processing type designation. For the samples with 0.5 and 1 wt.% content of TEG, XRD analysis was not performed since the carbon additive content is below the resolution limit of the technique

As seen from the figure, composites after synthesis and after HPT treatment at different temperatures demonstrate reflexes confirming the absence of reactions of Ni carbonyls/carbides as well as Ni-C solid solution formation during synthesis and annealing. The absence of carbon peak at $2\theta$=26.5° in all X-Ray patterns can be regarded as indirect evidence of complete carbon-containing phase incorporation into metallic matrix. It is interesting to note that in case of nanosized nickel as a starting material for nickel-graphene-graphite composite fabrication, such a reflex was observed in corresponding XRD patterns already at 1 wt.% content of carbon-containing phase. The observed difference is likely due to the fact that the surface area of nanonickel powder is much higher than for sieved fine-grained nickel powder affecting the size of coherent scattering regions [20]. HPT treatment at 6 GPa and *N*=10 turns favors specimens amorphization due to crystallites size decrease. Table 1 lists mean crystallite size estimated using Sherrer's equation and Voigt Function [21] in Specimens with 2 wt.% TEG before and after HPT. In case of Voigt Function estimation, the value of structural strain $\varepsilon$ was also calculated. Indeed, HPT at RT favors crystallites decrease in ~8-10 times. HPT at 200 °C results in some retardation of this effect, crystallite size here is 145 nm (estimates using Voigt Function). The difference between two estimation approaches for sample IV3 is, likely, related to strain value which is not accounted for in Sherrer's equation estimations.

**Table 1.** Mean size of crystallites estimated in composite specimens IV1-IV3 using Sherrer's equation and Voigt Function, as well as structure strain calculated in case of Voigt function method.

| | IV1 | IV2 | IV3 |
|---|---|---|---|
| *d*(Scherrer's) | 300 | 24 | 46 |
| *d*(Voigt function) | 303 | 35 | 145 |
| $\varepsilon$ (structure strain) | 0.002 | 0.009 | 0.05 |

*d* in nm, $\varepsilon$ in a.u.

Further analysis of carbon allotropes in composite Specimens with 0.5, 1, and 2 wt.% of graphene-graphite phase was carried out by Raman spectroscopy, see spectra of specimens I-IV in Fig. 4.

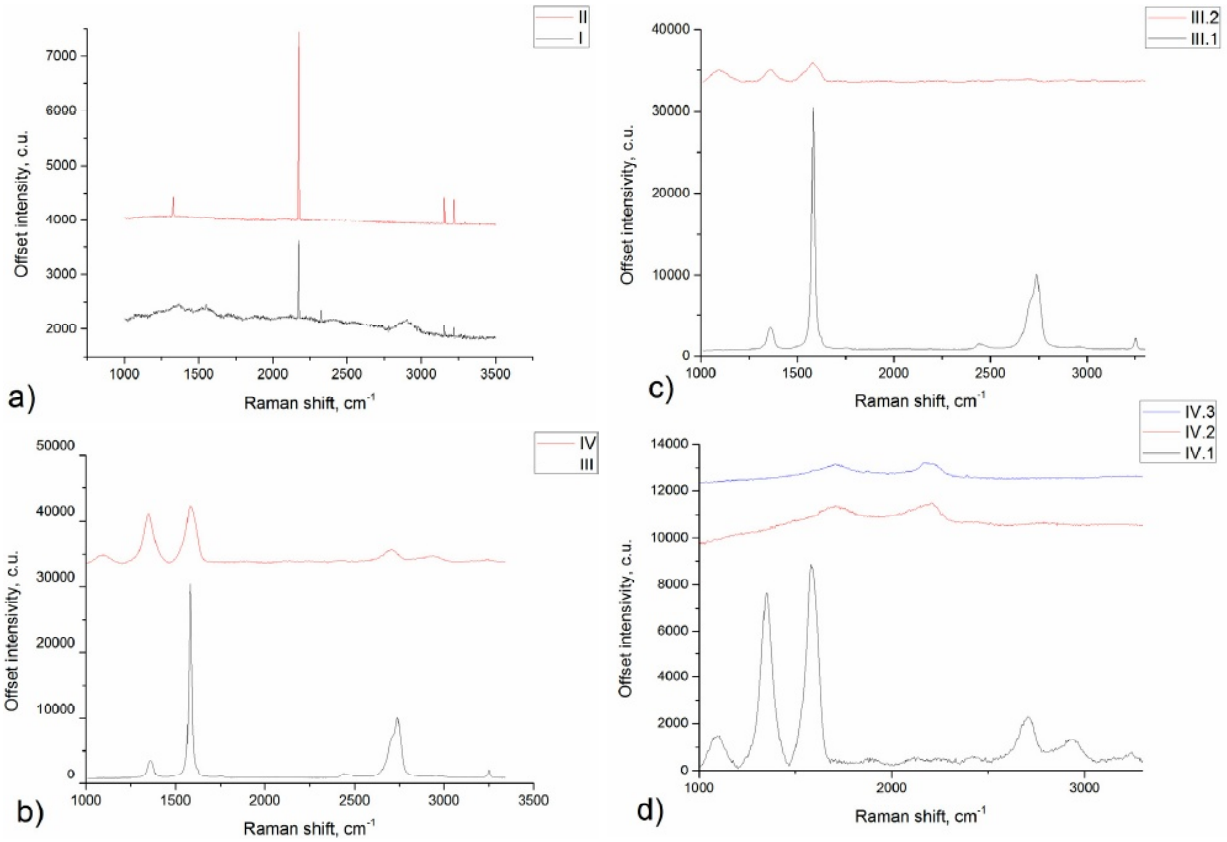


**Fig. 4.** Raman spectra of specimens (a) I and II before HPT (b) III and IV before HPT, (c) III before and after HPT at room conditions, (d) IV before and after HPT at different temperatures.

As shown in Fig. 4a, peaks corresponding to pure nickel are present in Raman spectra of Specimens I (pure nickel) and II, while the complete TEG to graphene conversion can be stated for Specimen III (see Fig. 4b). Since the intensity of G peak at 1578 $cm^{-1}$ in the spectrum of Specimen III is higher than that of 2D peak at 2880 $cm^{-1}$, one can conclude that the most part of graphene is present in a form of flakes with 6-8 layers in them. The presence of additional peaks at 2710 and 3550 $cm^{-1}$ is attributed to disordered flakes orientation. The increase of TEG content in the powder mixture over 1 wt.% results in the decrease in the graphene-to-graphite ratio in the manufactured composites. Latter is accompanied by distinct graphite region isolation. HPT treatment (Figs. 4c and 4d) results in complete 2D graphene structure destruction that manifests itself as a drastic decrease in Raman reflexes intensity, 2D peak is not observed here. It could be assumed that this 2D structure destruction is accompanied by the formation of some linear carbon polymers (like carbines) or by the destruction of hexagonal rings of graphene structure with its amorphization. It can be assumed that defects here are introduced into material during high pressure torsion, this assumption agrees with TEM observations.

Fig. 5 illustrates the comparison of TEM images taken for Specimen I without carbon-phase addition and Specimen III with (1 wt.% of graphene phase) before and after HPT at RT. Analyzing these images, one can conclude that specimens before HPT are microporous. Graphene addition results in significant pore size decrease. Also, pores shape tends to change towards cylindrical. HPT at RT leads to significant increase in the defect sizes, pore shape and their orientation change. Pores reorientation in the direction of material flow during HPT can be seen for Specimen III (see Fig. 5d). The increase of HPT temperature to 200 °C favored material porosity reduction. However, the deformation at elevated temperature does not eliminate it completely. Mention that the discussed TEM data agree with the results of density determination performed by hydrostatic weighing method. It is interesting to note that density change with deformation is non linear: it is 7.9, 8.2, and 7.8 $g/cm^3$ for Specimens IV1, IV2, and IV3, respectively. Some decrease in density observed for Specimen IV3 after HPT at 200 °C comparing to

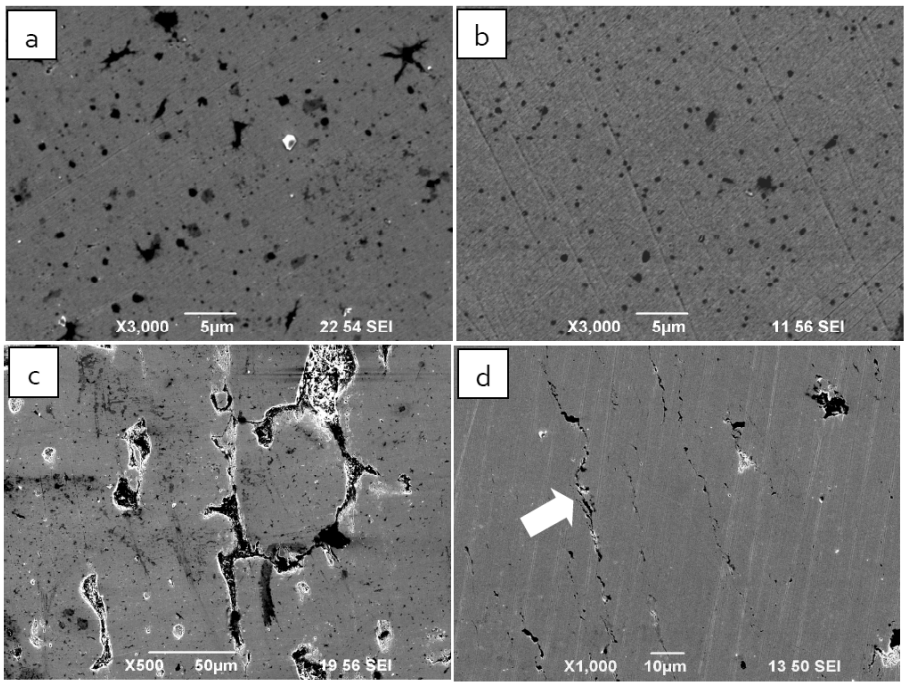


**Fig. 5.** Typical TEM microphotographs of specimen surface (a) I and (b) II before HPT and same specimens (c) I and (d) III after HPT at RT.

the non-deformed samples can be assumed as a result of closed pores appearance due to their reorientation and simultaneous crystallite and grain size change as a result of HPT treatment.

The results of microhardness measurements are presented in Fig. 6 and Table 2. Comparing these data, one can conclude that the increase in graphene-graphite phase content in the composites from 0.5 to 2 wt.% results in microhardbess increase. The most notable microhardness increment is noticed after HPT at RT. The results of mechanical testing of Specimens I-IV are shown in Table 3 and Fig. 7. The $\delta$ value change of Specimen I from 18 to 52% indicated a notable ductility of pure nickel (see Fig. 7a). In contrast, Specimens II-IV, containing graphite-graphene phase, showed brittle fracture character after HPT treatment at RT. The increase of HPT temperature for Specimen I resulted in the strength decrease and ductility increase (Fig. 7b). The increase of HPT temperature up to 200 °C did not significantly affect the discussed characteristics of Specimens II-IV, brittle fracture should be also mentioned.

It is interesting to compare the results of present work obtained for Specimen I (pure nickel without the deformation) with the data reported in [21] for nanocrystalline nickel (ncNi), obtained by electrical deposition (these data are also presented in Table 3). It should be noted that the value of tensile strength after fracture ($\sigma_b$) and ductility ($\delta$) of nickel, obtained by ball milling and powder metallurgy technique after HPT at RT are close to those for nc-Ni. Specimen I2 (HPT at RT) demonstrates tensile strength higher than 11 GPa and relative elongation to failure higher than 18%. Some difference in the nominal yield stress ($\sigma_{02}$) of pure nickel specimens, obtained by two different methods, can be explained as being due to developed structure of dislocations in the material after HPT. Specimens after HPT at 200 °C demonstrate the best combination of strength

**Table 2.** Microhardness (GPa) of specimens I-IV before and after HPT at different temperature regimes.

| deformation regime | Specimen | | | |
|---|---|---|---|---|
| | I | II | III | IV |
| no HPT | 1.56±0.19 | 1.96±0.25 | 1.97±0.17 | 2.24±0.15 |
| HPT at RT | 4.30±0.34 | 5.72±0.31 | 5.96±0.40 | 6.47±0.49 |
| HPT at 200 °C | 3.47±0.25 | 5.14±0.29 | - | 5.46±0.44 |

**Table 3.** Mechanical properties of specimens I-IV after strain tests at RT.

| Compostion | Deformation regime | Specimen number | $\sigma_{02}$,(GPa) | $\sigma_b$,(GPa) | $\delta$,(%) |
|---|---|---|---|---|---|
| I | HPT at RT | 1 | 1048 | 1201 | 1.8 |
| | | 2 | 884 | 1137 | 5.2 |
| | HPT at 200 °C | 1 | 923 | 992 | 9.9 |
| nc-Ni [20] | Initial state | - | 839 | 1233 | 3.0 |
| | Annealing at 200 °C | - | 604 | 1221 | 7.1 |
| | Annealing at 300 °C | - | 141 | - | |
| II | HPT at RT | 1 | 277* | - | |
| | | 2 | 471* | - | |
| | HPT at 200 °C | 1 | 575* | - | |
| | | 2 | 343* | - | |
| III | HPT at RT | 1 | 193* | - | |
| | | 2 | 177* | - | |
| IV | HPT at RT | 1 | 130* | - | |
| | | 2 | 248* | - | |
| | HPT at 200 °C | 1 | 784* | - | |
| | | 2 | 107* | - | |

* - stress fracture

($\sigma_{02}$= 923 MPa, $\sigma_B$= 992 MPa) and ductility ($\delta$ = 99%). However, according to the shape of "stress-strain" curves, the plasticity mechanism in HPT-treated samples is realized mainly due to the specific localization of the deformations.

In order to study the origin of the mentioned difference in mechanical behavior of HPT-treated Specimens I-IV, the analysis of fractured surface after elongation has been performed. TEM images of fractured surface of HPT treated Specimen I (pure nickel) demonstrated ductility, while brittle fracture was confirmed for HPT treated samples containing graphene-graphite phase (Fig. 8). Figs. 8a-8d demonstrate an evident cross section decrease in case of Specimen I. At the same time, the cross section does not change for composites after brittle failure. The significant difference in the fracture character can be observed in Figs. 8b and 8e. Fracture picture observed for Specimen IV is typical for the highly strengthened materials with the high crystalline defects concentration introduced by deformation: grain boundaries, lattice dislocations, nanosized segregations formed by impurity atoms, etc. Dimpled fracture is mainly observed in Specimen I with the dimple size being 150-400 nm. Dimple depth gives an evidence that the material possesses low ductility. The dimples formed on the fractured surface of Specimen IV are smaller by an order of magnitude and possess lower depth. In addition, flat regions of poorly defined relief are present on the fractured surface of bulk "nickel-graphene-graphite" composites, this is typical for brittle materials. Numerous secondary branches from the main crack are also registered on the fractured surface (indicated by arrows in Fig. 8a). That supports the conclusion on possible secondary cracks formation nucleated in pores (see Fig. 5).

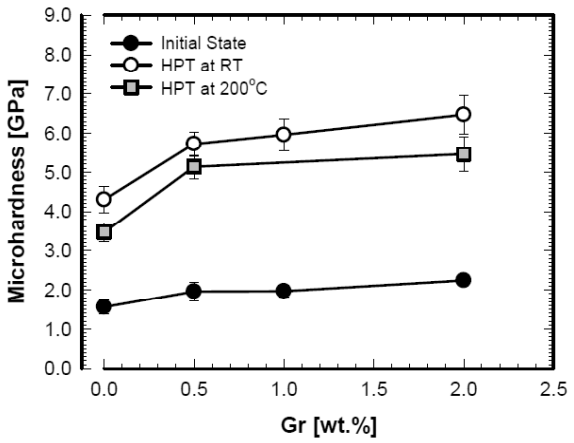


**Fig. 6.** The dependence of specimens microhardness on TEG addition and HPT regime.

From the data above, one can conclude that the presence of microsized defects (pores) can be regarded as one of the driving factors of brittle fracture

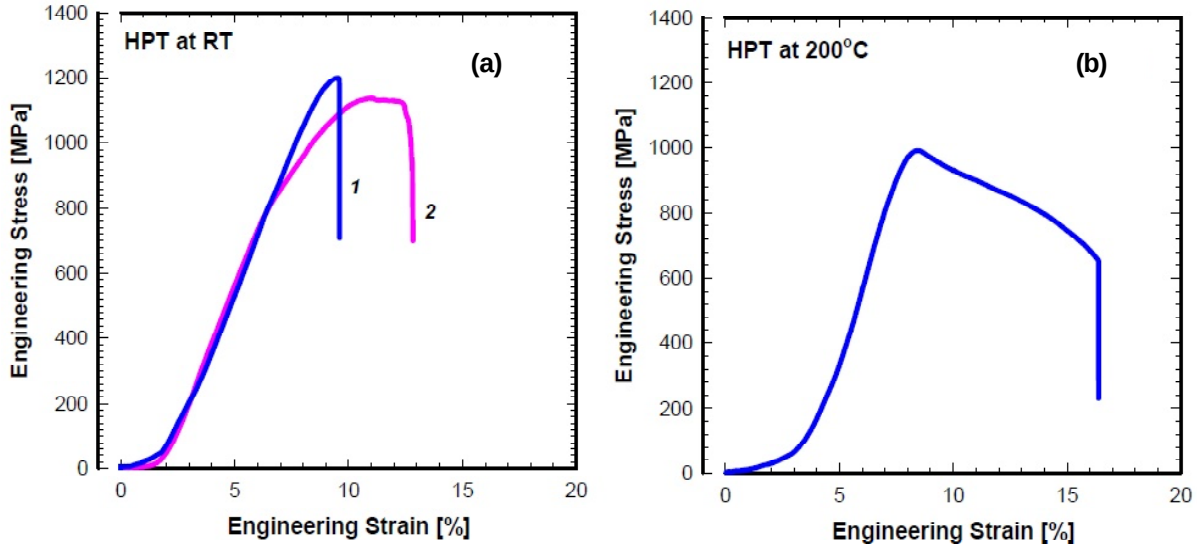


**Fig. 7.** The results of mechanical tests.

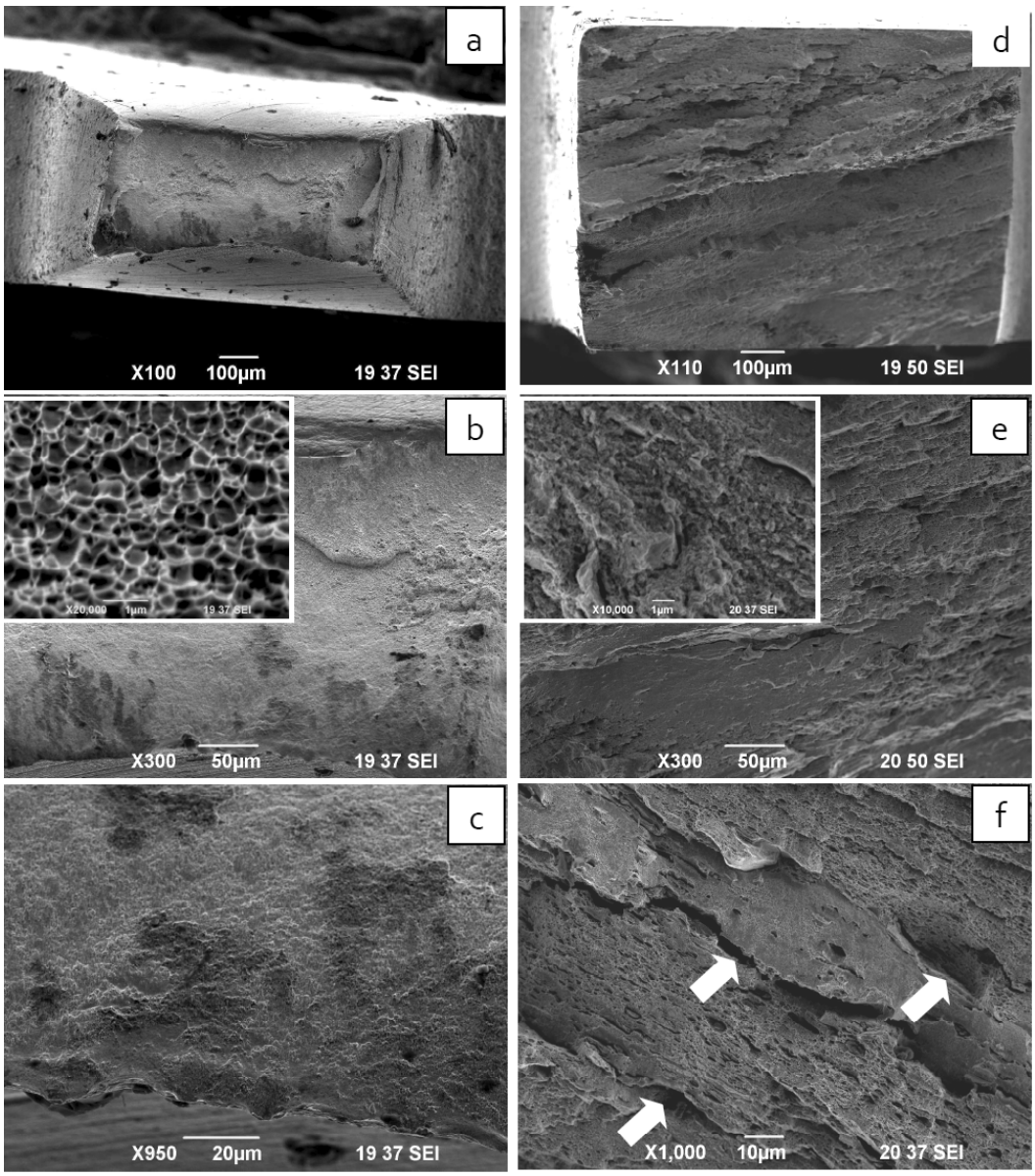


**Fig. 8.** Typical TEM images of sample fracture taken for specimens HPT treated at RT: Specimen I (a-c) and Specimen IV (d-f) after their failure during the elongation tests.

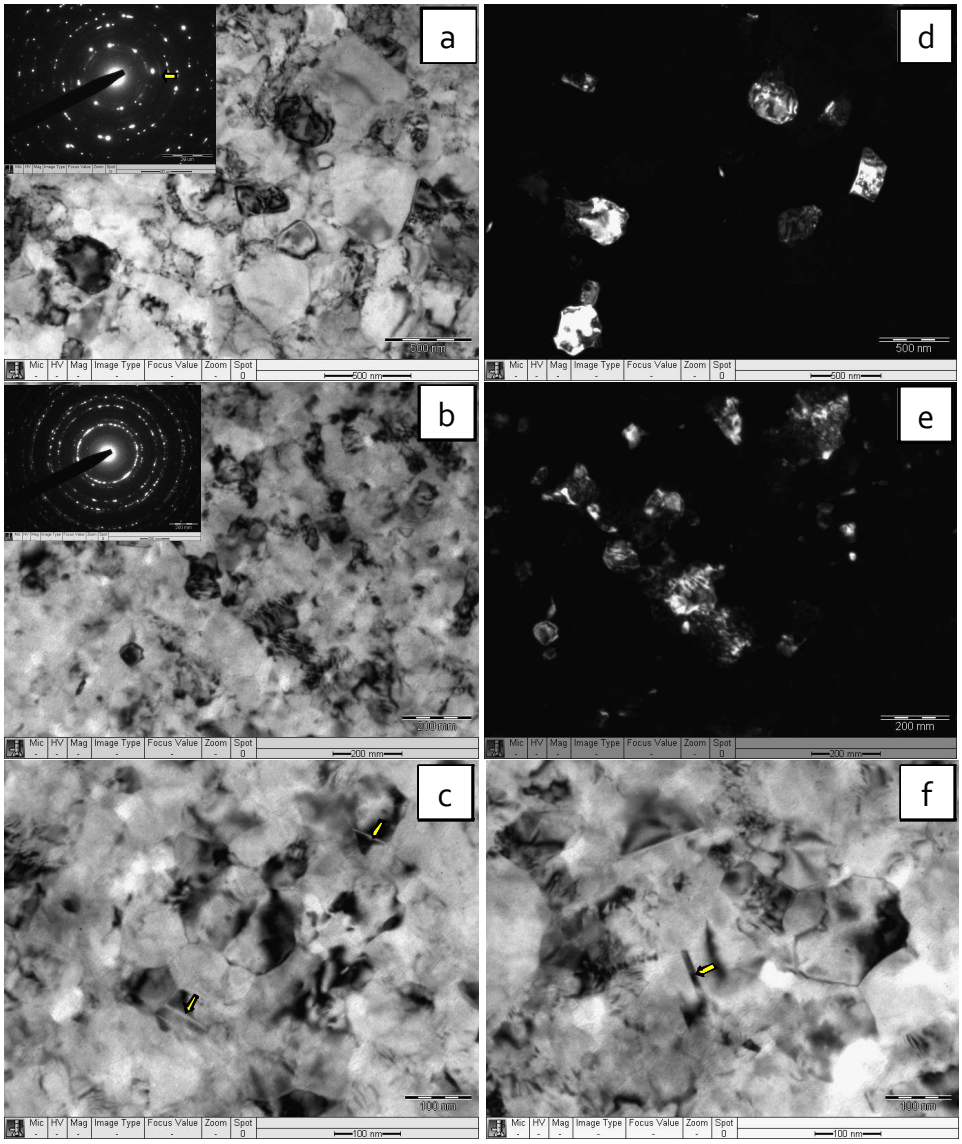


**Fig. 9.** Typical microstructure of Specimen I1 (a,b) and Specimen IV3 (c-f). The inserts in Fig. (a, c) are the diffraction patterns from selected regions of the microstructure.

of nickel-graphite-graphene composites. The fracture process is initiated there at relatively low applied load. The formation of nanosized allocations or segregations composed of impurities atoms, formed during deformation process are likely a cause of low ductility (brittle fracture) of HPT deformed composites II-IV. Such impurities redistribution can be possible during annealing, see, e.g. [21]. Moreover, the investigation of some iron, aluminum, and nickel-based alloys with insignificant carbon content shows that grain boundaries atoms segregations of alloying elements are induced by HPT treatment. Latter can be due to diffusion activation causing the vacations generation [9,22]. However, further microstructure investigation should be undertaken to prove this assumption.

In order to clarify the observed increased strength values obtained for HPT treated samples (see Figs. 5 and 6, Tables 2 and 3), their microstructure was examined by TEM. Typical images of structures formed in Specimens as a result of HPT treatment are shown in Fig. 9. As seen from the figure, HPT processing favors the ultrafine structure formation both in pure nickel specimens and nickel-graphene-graphite composites. That structure is typical for metallic and composite materials after severe plastic deformation (SPD) [16].The type of diffraction patterns in Figs. 9a and 9c indicates that grain boundaries formed have mostly high angled

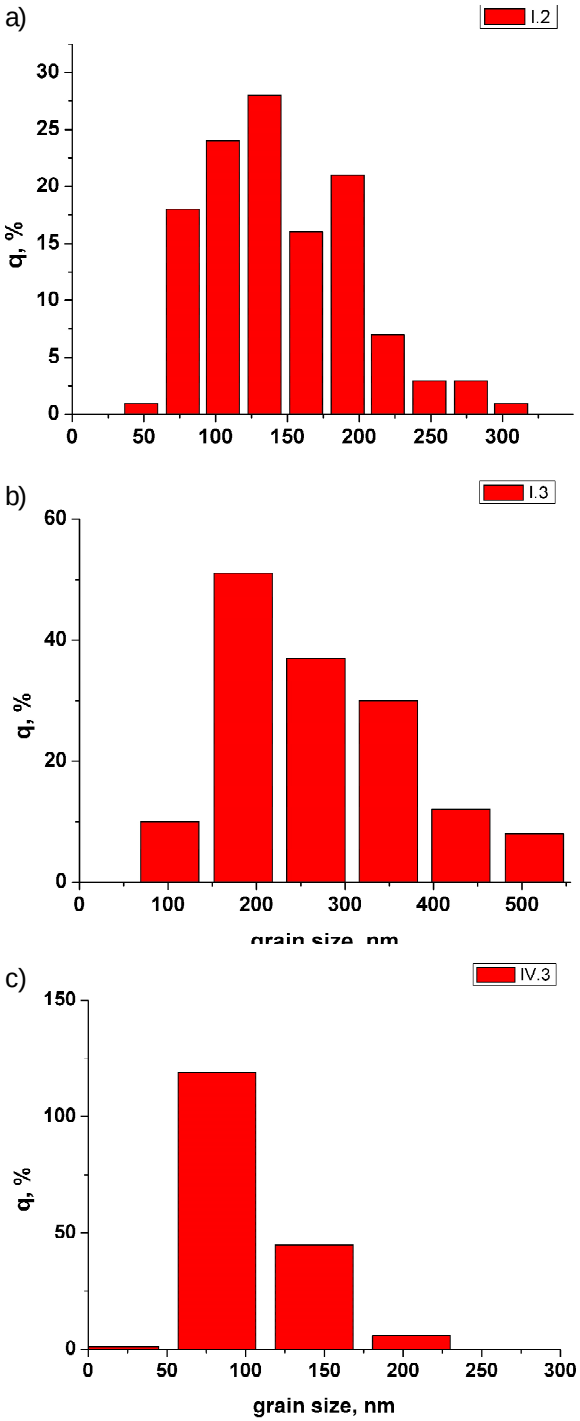


**Fig. 10.** Grain size distributions in Specimens (a) I2, (b) IV2, and (c) IV3.

misorientations Nanosized twinning is observed along with ultrafine grains formation (see arrows in Figs. 9e and 9f). The grain size distributions are obtained from the quantitative grain size analysis performed for pure nickel specimens and nickel-graphene-graphite composites (results based on TEM data of 60-80 grains measurements, Fig. 10). The grain size in specimens after HPT at RT and at 200 °C varies from 50 to 300 nm. The increase of HPT temperature results in the grain size increase from 123 to 184 nm. The incorporation of graphite-graphene mixture results in mean grain size decrease to 102 nm and overall distribution narrowing. The tendency is in accordance with crystallites size change in specimens under different HPT treatment regimes obtained for Specimen IV (see Table 1).

## 4. CONCLUSIONS

For the first time, bulk nickel and nickel-graphene-graphite composites with 0.5-2 wt.% of graphite-graphene phase content were manufactured by high energy ball milling and powder metallurgy techniques. Raman spectroscopy showed that complete graphite to graphene conversion is observed only in case of 1 wt.% of graphite-graphene phase content. Mechanical testing revealed that microhardness of the specimens increases with the increase in graphite-graphene mixture content. HPT treatment at room temperature favors to microhardness increase in 3 times. Due to significant residual porosity of all bulk nickel-graphene-graphite composites, their brittle fracture upon elongation in the elastic region was observed regardless HPT treatment regime. HPT treatment results in pores redistribution and reorientation, ultrafine grains structure formation, and nanotwinning

## ACKNOWLEDGEMENTS

This work was supported by the Russian Science Foundation (project 14-29-00199). Raman spectroscopy research was performed at the Center for Optical and Laser Materials Research at Research park in St Petersburg State University.

## REFERENCES

[1] S.C. Tjong // *Materials Science and Engineering: R: Reports* **74** (2013) 281.
[2] J.A. Hooker and P.J. Doorbar // *Materials science and technology* **16** (2000) 725.
[3] A.F. Zimmerman, G. Palumbo, K.T. Aust and U. Erb // *Materials Science and Engineering: A* **328** (2002) 137.
[4] P. Narasimman, M. Pushpavanam and V.M. Periasamy // *Wear* **292** (2012) 197.

[5] D.D. Roshan // *IEM Journal of R & D* **22** (1978) 681.
[6] J. Zahavi and J. Hazan // *Plat Surf Fin* **21** (1983) 57.
[7] X.H. Chen, C.S. Chen, H.N. Xiao, F.Q. Cheng, G. Zhang and G.J. Yi // *Surface and Coatings Technology* **191** (2005) 356.
[8] X.H. Chen, J.C. Peng, X.Q. Li, F.M. Deng, J.X. Wang and W.Z. Li // *Journal of Materials Science Letters* **20** (2001) 2057.
[9] G.B. Rathmayr and R. Pippan // *Acta materialia* **59** (2011) 7228.
[10] C. Zhao // *Applied Physics* A **118** (2015) 409.
[11] D. Kuang, L. Xu, L. Liu, W. Hu and Y. Wu // *Applied Surface Science* **273** (2013) 484.
[12] T. Borkar, H. Mohseni, J. Hwang, T.W. Scharf, J.S. Tiley, S.H. Hong and R. Banerjee // *Journal of Alloys and Compounds* **646** (2015) 135.
[13] B. Yang and H. Vehoff // *Materials Science and Engineering: A* **400** (2005) 467.
[14] V.G. Konakov, I.A. Ovid'ko, N.V. Borisova, E.N. Solovyeva, S.N. Golubev, O.Yu. Kurapova, N.N. Novik and I.Yu. Archakov // *Rev Adv Mater Sci* **39** (2014) 41.
[15] A. Vorhauer and R. Pippan // *Scripta Mater* **51** (2004) 921.
[16] A.P. Zhilyaev and T.G. Langdon // *Prog Mater Sci* **53** (2008) 893.
[17] Russian State Standard No 1497-84, *Metals The methods of the elongation testing.*
[18] E.C. Moreno-Valle, I. Sabirov, M.T. Perez-Prado, M.Yu. Murashkin, E.V. Bobruk and R.Z. Valiev // *Mater Let* **65** (2011) 2917.
[19] M.Yu. Murashkin, I. Sabirov, A.E. Medvedev, N.A. Enikeev, W. Lefebvre, R.Z. Valiev and X. Sauvage // *Mater Design* **90** (2016) 433.
[20] V.G. Konakov, O.Yu. Kurapova, I.V. Lomakin, N.N. Novik, S.N. Sergeev, E.N. Solovyeva, A.P. Zhilyaev, I.Yu. Archakov and I.A. Ovid'ko // *Rev Adv Mater Sci* **50** (2017) 1.
[21] T.H. De Keijser, J.I. Langford, E.J. Mittemeijerand and A.B.P. Vogels // *J Appl Cryst* **15** (1982) 308.
[22] Y.M. Wang, S. Cheng, Q.M. Wei, E.Ma, T.G. Nieh and A. Hamza // *Scr Mater* **51** (2004) 1023.
[23] I. Sabirov, N.A. Enikeev, M.Yu. Murashkin and R.Z. Valiev, *Bulk Nanostructured Materials with Multifunctional Properties* (Springer Briefs in Materials, 2015), DOI 101007/978-3-319-19599-5.